Ergonomic Path Planning for Autonomous Vehicles-An Investigation on the Effect of Transition Curves on Motion Sickness

Siddiqi, Muhammad Rehan; Alamdari Milani, Sina; Nakhaie Jazar, Reza; Marzbani, Hormoz

Siddiqi, M. R., Alamdari Milani, S., Nakhaie Jazar, R., & Marzbani, H. (2022). Ergonomic Path Planning for Autonomous Vehicles-An Investigation on the Effect of Transition Curves on Motion Sickness. IEEE Transactions on Intelligent Transportation Systems, 23(7), 7258–7269.
https://doi.org/10.1109/TITS.2021.3067858
Document Version: Accepted Manuscript

Published Version: https://doi.org/10.1109/TITS.2021.3067858

Ergonomic Path Planning for Autonomous Vehicles - An investigation on the effect of transition curves on motion sickness

Muhammad Rehan Siddiqi, Sina Milani, Reza N.Jazar, Hormoz Marzbani

***Abstract*—Motion sickness in self-driving cars is a key human factor that aggravates the passengers' health in autonomous vehicles and is investigated in the following pages. As drivers turn into passengers and passengers dwell into other activities, the probability of car sickness is inevitable in self-driving cars. Path planning could serve an important role in reducing sickness. The present study establishes thresholds that contribute to motion sickness from a vehicle's dynamic point of view to generate at first the most susceptible reference track to motion sickness, then redesigned using B-spline, Bezier, and Hermite curves to investigate the thresholds. Trajectory tracking of an eight degree of freedom vehicle model within the Autodriver algorithm is then studied using curvature dependent and curvature independent controllers to draw a comparison. Results are then compared and evaluated to find the optimal transition curve to minimize motion sickness probability. Furthermore, the findings are applied to lane changing maneuvers using various transition curves. Results indicate that four out of five of the motion sickness thresholds were successfully addressed in this investigation. Further research is recommended to address the fifth motion sickness threshold by utilizing the transition curve's key characteristics like local control and non-uniformity.**

***Index Terms*— Autonomous Vehicles, Transition curves, Path Planning, Motion Sickness, Autodriver Algorithm, Ergonomic path planning, motion planning and Road Design.**

List of Symbols

$v_{x,y}$	Longitudinal and lateral velocities in vehicle body frame
β	Vehicle side-slip angle
ψ	Yaw (heading) angle
r	Yaw rate
ϕ	Roll angle
p	Roll rate
s	Path-tracking error
κ	Curvature
ρ	Radius of curvature
m	Vehicle mass
$a_{1,2}$	Distance from mass center fo front and rear axles
$C_{\alpha_{f,r}}$	Tire cornering stiffness at front and rear
$C_{T_{f,r}}$	Roll torque coefficient at front and rear
$C_{\beta_{f,r}}$	Wheel-slip coefficient at front and rear
$C_{\delta_{\phi f,r}}$	Roll-steer coefficient at front and rear
$C_{\phi_{f,r}}$	Camber thrust coefficient at front and rear
c_ϕ, k_ϕ	Roll damping and roll stiffness coefficients
$I_{x,z}$	Roll and yaw mass moments of inertia
δ	Steering angle
F_x	Longitudinal force
X, Y	Global coordinates of the mass center
$C_{r,p,\beta,\phi,\delta}$	Force system coefficients of lateral equation
$D_{r,p,\beta,\phi,\delta}$	Force system coefficients of yaw equation
$E_{r,p,\beta,\phi,\delta}$	Force system coefficients of roll equation
S_κ, S_β, S_r	Steady-state curvature, side-slip and yaw-rate responses
${}^G\mathbf{r}$	Vector $\vec{r}$ expressed in frame G
T	Wheel torque
R_w	Wheel radius
R	Road radius of curvature

I. Introduction

A few automation levels have already been introduced to vehicles, such as forward collision warning, adaptive cruise control, and lane-keeping to fully automated driving. The Society of Automotive Engineers have classified automation into 6 distinctive levels; level zero indicates the absence of automation; level one indicates a single task being automated; level two has at least two or more tasks automated; level three is where the vehicle handles dynamic driving tasks; level four where cars are officially driverless and level 5 vehicles are entirely autonomous,[1] with self-driving cars having the potential to lead to significant benefits, such as increased comfort and productivity.

The introduction of such systems has raised several classic human factor issues, [2]. Of-particular immediate concerns are the questions that arise at automation level 3 known as Conditional Automation. The driver is expected to resume vehicle control with a sufficiently comfortable transition time in case the system reaches its performance limits; or because the driver desires to return to manual drive. The safe and comfortable transitioning between in-the-loop and out-of-the-loop behaviours raises several questions, [2]. In a more general sense, the fact that the passengers of such vehicles face a loss of control has also raised more human factor questions such as loss of control-ability [3], [4].

However, the integral point of discussion in this study is the fact that most of the envisaged scenarios lead to an increased risk of motion sickness [5]. This can negatively affect user acceptance, uptake, and, in turn, limit the potential socioeconomic benefits that this emerging technology may provide. Hence, the present study provides a practical solution to resolve the problem of motion sickness in autonomous vehicles because of self-driving technology.

The remaining structure of the paper is as follows: In section 2, a review of the previous work done for passenger comfort with more emphasis on the background of motion sickness theories, its impacts on passenger cars and their measuring techniques are mentioned. In section 3, the problem is defined and the methodology used in the study is discussed. In section 4, the details of the architecture of the path tracking controller are explained. In section 5, the simulation strategy and tools for investigating the problem are introduced. In section 6, analysis of transition curves and their thresholds are shown for a particular point selection. In section 7, mid-point optimization is illustrated to limit motion sickness and finally the conclusion and discussions for future work are presented in section 8.

II. Related Works

Passenger comfort in ground transportation is determined by the changes in the motion felt in all directions [3]. Studies that focused on the comfort levels in the longitudinal direction are limited to acceleration or jerk motion while ignoring lateral motion [6]. Bellem investigated comfort in autonomous driving by studying different driving scenarios [7]. Authors in [8] introduced definition for human-comfort in autonomous driving for passenger vehicle navigation based on electric wheelchair experimentation. Human comfort in terms of enhancing the controller was discussed and optimized in [9]. A cost function was developed based on five factors and investigated by root mean square (RMS) and Fast Fourier Transforms (FFT). The cost function was then used to optimize the controller to follow a clothoid path. However, one human factor was never addressed until Diels [5] raised the issue that vehicle automation can increase the likelihood and severity of motion-sickness. The reason is that scenarios envisaged for self-driving cars create conditions that promote the incidence and severity of motion sickness. Generally speaking, incongruities between what is felt versus seen typically aggravates symptoms, whereas looking at the earth-fixed horizon, even when it is presented artificially, may be beneficial [10][11][12]. Other researches proved that in-vehicle entertainment systems can increase the incidence and severity of carsickness and decrease situation awareness [13][14].

To define the problem, the next few sections elaborate the most well known theories of motion sickness, followed by an in-depth understanding of the impact it has on passenger cars, with lastly over viewing the techniques used for measuring motion sickness.

A. Motion Sickness Theories

The most common hypothesis of motion sickness is the Treisman poison theory that defines motion sickness as a defense mechanism against neurotoxins [15]. The brain concludes that if motion is perceived and not visualized, or vice versa, this discordance is believed to be a poison ingested into the control system, resulting in inducing the action of vomiting.

A more definitive theory addressed by Reason and Brand in [16], called the "motion sickness theory" states that motion sickness is an occurrence between the conflict of senses and stored patterns of motion reference. The theory served as the basis of understanding how the three responsible sensors for balance and control (vestibular system, vision and somatosensory system) interact with our central nervous system.

Although the theory holds for most of the scenarios but Riccio and Stoffregen supported by their investigation in [17], stated the theory of motion sickness was more hypothetical than reality. They introduced the "postural instability theory", which states that postural instability is a necessary and sufficient condition preceding motion sickness. However, this theory was discredited by Bos in [18] stating instances where motion sickness existed and postural instability did not and vice versa. The study supported for the theory presented by Kennedy and Stanney [19], which states that both motion sickness, and postural instability are second order effects with a common centre.

B. Motion Sickness in Passenger Cars

In [20], Griffin delivered extensive research to investigate the factors causing motion sickness in ground transportation, considering motion in all directions. In [21], roll and pitch oscillations are extensively investigated. Motion sickness by combined lateral and roll oscillation [22] is also investigated by studying the effect of varying phase relationships. In [23], the effect of driver, route, and vehicle type on the causation of motion sickness are studied. Further support of work is presented in [20], where four different experiments were utilized to interpret vehicle motion's effect on motion sickness. All results showed conclusive evidence of low-frequency lateral and longitudinal acceleration as the dominant cause of motion sickness in passenger cars. The primary factor influencing these vehicle forces was the driver. The driver's ability to take smoother turns and gradual acceleration and deceleration lead to lower motion sickness in passengers.

In [24], motion sickness was investigated in a test track with equal turns and braking events, under moderate and low accelerations. At the same time passengers were engaged once; in a task and once without a task. Motion sickness ratings of passengers were based on a motion sickness questionnaire ranging from a scale of zero to ten, where a rating of ten constitutes the highest level of sickness. Moderate acceleration, together with a task being performed by passengers, caused the highest level of motion sickness rating in passengers. The Influence of lateral, roll and motion gains on the driving performance of an advanced dynamic simulator on a slalom track was studied in [25]. All-inclusive, the level of motion sickness was highest when the advanced simulator had the highest lateral motion gain associated with the dynamic simulator.

According to the studies in [26], [27], [28], the level of comfort corresponded to a threshold value of comfort at $1.8m/s^2$, while medium comfort and discomfort levels were evaluated at $3.6m/s^2$ and $5m/s^2$, respectively. The lateral acceleration of cars was measured on Chinese highways in [29] and a smaller radius of turning was reported as the primary reason for higher discomfort levels.

Over all the above works mentioned, indicate a very strong correlation of motion sickness with high magnitude low-frequency roll and lateral accelerations. Additionally, the above mentioned studies have adopted variant tools to measure motion sickness in their studies, some of which have been mentioned in the following section.

C. Modes of Measuring Motion Sickness

One of the earliest questionnaires used was the Pensacola Motion Sickness Questionnaire (MSQ) [30], which allowed subjects to identify their symptoms during experimentation. Another well-known questionnaire used for simulator experiments is the Simulator Sickness Questionnaire (SSQ), which allowed simulator participants to identify sickness symptoms they felt during simulations [31], [32], [33], [34], [35].

Other techniques to quantify motion sickness have been defined in British standard 6841 [36] and International Standard 2631 [37], such as the use of Motion Sickness Dosage Value (MSDV), which is the frequency weighted acceleration of the vehicle utilized in many studies for measuring motion sickness [20], [38], [39], [40], [41]. Many clinical studies utilize Electroencephalography (EEG) [42], [43], [44], [45], which is the measurement of cerebral changes when a participant undergoes motion sickness stimulus, showing which parts of the human brain become the most active during motion sickness. Currently, mathematical models have been successfully used to identify key aspects of motion sickness. Subjective Vertical Conflict (SVC) was used to identify the Motion Sickness Incidence (MSI) in a driver, and the passenger of a car due to the changes in their head tilt angles [46].

The present study conducts extensive research for finding the motion sickness thresholds, which are then utilized to design a reference track based on straight lines and circular arcs, labelled as the ”Worst path”. The Worst path is then manipulated with three transition curves, namely the Hermite, Bezier, and B-spline, to undergo various scenarios for simulation using the Autodriver algorithm, combined with Sliding Mode Controller (SMC) and Model Predictive Controller (MPC) as trajectory tracking mechanisms. The resultant vehicle motions are then discussed and compared with respect to the defined motion sickness thresholds identified in this study. The sections to follow, define the problem addressed in this study, followed by a detail look into the path tracking mechanisms and motion planning simulations utilized to resolve this problem.

III. Problem Statement

The mentioned studies indicate a broad knowledge of motion sickness contributing factors, but none of the studies present a solution or strategy to solve the problems faced by passengers due to motion sickness. Additionally, most of the modes of measuring are either subjective or generic. Our study analyzes the problem of motion sickness in passengers of Autonomous Vehicles by individually addressing key vehicle-driven parameters contributing to motion sickness in passengers. These five key parameters have been labelled as ”Motion Sickness Thresholds”, and are summarized below:

- A track which produces abrupt lateral acceleration over the range of discomfort as defined in [26], [27], [28].
- A track producing high-magnitude low-frequency lateral accelerations during cornering maneuvers, as mentioned in [20], [23] . The peak of sickness probability occurs at $0.16Hz$, while frequencies above $1Hz$ cause no sickness [5]. Thus, the range of frequency to evaluate the motion sickness in a path is in the range of $0.1Hz - 0.2Hz$.
- A track during which the lateral acceleration and roll oscillations are in phase, [22].
- Abrupt changes in velocity and steering input during the travel [47], [48], [49].
- A track produces successive turns in opposing directions [50].

In the following sections, through critical analysis of these thresholds, we will present the best possible path to limit, avoid, or minimize motion sickness in passengers.

IV. Path-tracking control

To enable the study of path-planning methodologies on motion sickness, a path-tracking platform is needed in order to keep the ego vehicle as close as possible to the designed target path. No controller can guarantee exact path-tracking; however, we may initiate a systematic comparison on the path-planning methodologies by adopting a standard path-tracking approach to act as the benchmark for this analysis. The sliding mode controller works based on Autodriver algorithm as a feedforward structure, which is explained first; the model-predictive controller is considered as well, due to its popularity and proven performance in path-tracking applications. Comparing these two approaches provides us with more generic conclusions on the resulted motion sickness.

A. Autodriver algorithm

Employing the concept of center and radius of curvature of the road, and the dynamic rotation center of the vehicle, [51] introduced a method for calculating the required steer angle to keep the vehicle on the given road . This is done by coinciding the center of curvature of the vehicle and the road. The algorithm was later developed to use simpler methods for calculating steering angles where close-to-dynamically-precise steering angles could be produced using simple kinematic equations [52]. The algorithm was farther equipped with control mechanisms to assure a practical approach [53].

To apply the Autodriver algorithm as a trajectory tracking mechanism, the desired path of motion given as a mathematical equation is needed.

$$\dot{v}_x = \frac{F_x}{m} + r v_y, \tag{1}$$

$$\dot{v}_y = \left(\frac{C_r}{m} - v_x\right) + \frac{C_p}{m}p + \frac{C_\beta}{m}\frac{v_y}{v_x} + \frac{C_\phi}{m}\phi + \frac{C_\delta}{m}\delta, \tag{2}$$

$$\dot{p} = \frac{1}{I_x}\left(E_r r + E_p p + E_\beta \frac{v_y}{v_x} + E_\phi \phi + E_\delta \delta\right), \tag{3}$$

$$\dot{r} = \frac{1}{I_z}\left(D_r r + D_p p + D_\beta \frac{v_y}{v_x} + D_\phi \phi + D_\delta \delta\right). \tag{4}$$

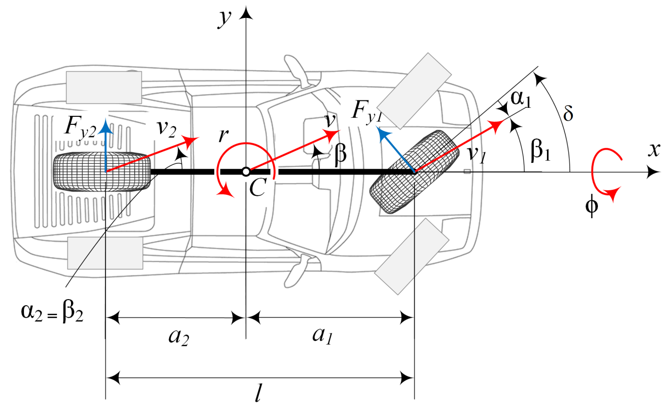

Fig. 1. Bicycle-Roll Vehicle Model

in which $C_{r,p,\beta,\phi,\delta}$, $D_{r,p,\beta,\phi,\delta}$, $E_{r,p,\beta,\phi,\delta}$ are the force system coefficients, introduced to simplify the equations. These coefficients are functions of the vehicle parameters listed in Table II, and they relate the external forces and moments to the kinematic variables of the vehicle. The complete list of these coefficients are found in [54].

The input to the system is steering angle δ. Forward velocity is assumed to be a parameter for a third-order system constructed by Equations (2-4). The tire forces are assumed to be proportional to the side-slip angles. Also, a single-track layout is assumed, which considers the effect of the left and right tires by using a single equivalent tire in the middle of the axle.

Later a technique called steady-state dynamic steering was introduced, which is based on the use of the steady-state responses of the vehicle [52], [55]. The steady-state curvature, yaw rate, and side-slip responses are used to formulate the Autodriver algorithm using the bicycle-roll model.

$$S_\kappa = \frac{\kappa}{\delta} = \frac{1}{\rho\delta}, \tag{5}$$

$$S_r = \frac{r}{\delta} = \frac{\kappa}{\delta} v_x, \tag{6}$$

$$S_\beta = \frac{\beta}{\delta} = \frac{v_y}{v_x \delta}, \tag{7}$$

Full expressions of the steady-state responses may be found in [56]. The Autodriver algorithm uses the fact that a vehicle on the road must always rotate about the center of curvature of that road to coincide with the center of rotation of the vehicle. Knowing the mathematical equation of any road as a spatial curve ($\vec{r} = \vec{r}(X, Y, Z, \psi)$) enables the calculation of the path of curvature center in the osculation plane, in global and vehicle body coordinate frames, [54]. Assuming there is no initial position error between the vehicle and the road, if the location of the road curvature center coincides with the vehicles rotation center at every instance, the vehicle will remain on the road. To compensate for transient errors and any uncertainties in modeling, corrective input steering δ, and v_x are selected.

The turning radius of the vehicle is mainly determined by the steering angle. Although the velocity does contribute to the location of Instantaneous Center of Rotation (ICR), it is less effective in determining the turning radius, especially at small side-slip angles [57]. Hence, the main factor determining the radius of rotation of the vehicle is assumed to be the steering angle. Thus, the aim is to set the steering angle to eliminate the position error between the ICR and the road curvature center laterally. The desired velocity is normally given by the high-level path planner as a velocity profile for different road sections.

B. Control Strategy

The path-tracking is realized by two different control strategies, namely a feedforward-feedback control with the aid of the Autodriver algorithm together with Sliding-Mode Control (SMC) technique, and a Model Predictive Controller (MPC). These strategies are chosen as they have been proven effective both in terms of control performance and real-time applicability [53], [56]. Although the controller design is not the main focus of this paper, a brief discussion on the control strategies is given in this section to elaborate on the path-tracking strategy; further details on the Autodriver algorithm and the controller design could be found in [53] and [56].

1) Longitudinal closed-loop control: The longitudinal control in both methods is performed using a Proportional-Derivative (PD) controller that eliminates the longitudinal position errors. The control input to the system in this direction is the longitudinal force F_x. Integral control is not considered here, because the controlled variable has a dimension of length (position), which inherently integrates the velocity as the manipulated variable. The calculated longitudinal force is converted to a torque input to the driving wheels with the simplified relationship:

$$T = F_x R_w. \tag{8}$$

2) Lateral control using SMC: The first strategy used for steering the vehicle onto the desired track (lateral control) is based on a feedforward-feedback strategy which uses the Autodriver algorithm as the feedforward section; this provides the main portion of the required steering angle when the vehicle enters a turn. However, the Autodriver algorithm is based on the steady-state vehicle dynamics which may lead to transient tracking errors. To eliminate such an error, a SMC feedback loop is added. The lateral tracking error dynamics is modelled based on an augmented bicycle model [58] which incorporates the lateral tracking error and its rate as state variables. The control law is derived as [56]:

$$\delta_{fb} = \delta_{eq} - k.\text{sat}\left(\frac{s}{\Phi}\right) \tag{9}$$

where,

$$\delta_{eq} = -\frac{C_{\alpha f} + C_{\alpha r}}{C_{\alpha f} v_x} v_y + \left(\frac{-a_1 C_{\alpha f} + a_2 C_{\alpha r}}{C_{\alpha f} v_x}\right) r + \lambda \dot{e}, \tag{10}$$

$$\text{sat}(u) = f(x) = \begin{cases} u, & |u| \leq 1. \\ \text{sgn}(u), & |u| > 1. \end{cases} \tag{11}$$

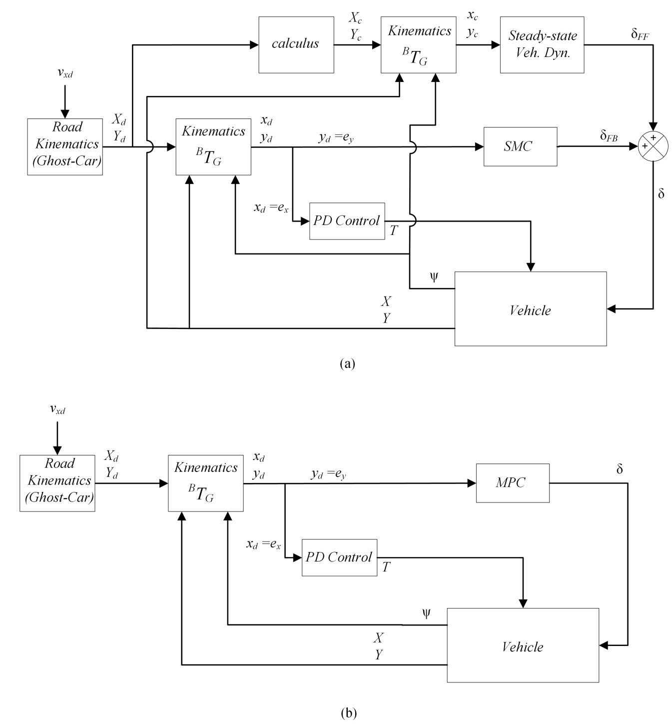

Fig. 2. Block-diagram of the control system: (a) SMC, (b) MPC

The vehicle is assumed to be working in normal driving conditions a low tire slip and tire forces well-below their saturation threshold. Controller parameters λ, k, Φ were initially tuned based on Figure 1 and lane-change scenarios using clothoids as transition curves, and they have been selected such that the controller satisfies the sliding condition for tire parameter uncertainties of up to 10%; the corresponding controller is referred to as ”SMC” in this text. Another tuning was later performed for a more aggressive controller based on a wider set of transition curves. The corresponding controller is referred to as ”SMC-Modified”. These two variants are used here with differently tuned parameters to observe the difference in the motion-sickness thresholds.

3) Lateral control using MPC: To compare the effect of transition curves on control performance and passenger comfort, a Model-Predictive Controller (MPC) is built as the internal model. The implementation is performed in MATLAB Simulink using the ”MPsee” toolbox [59], which utilizes the Generalized Minimum Residual Method (GMRES) as the optimization tool. A prediction horizon of 10 with a sampling time of $0.1s$ is considered for the MPC. A summation with counter k from 1 to 10 is needed over e_k and δ_k. The cost function and constraints are considered as [56]:

$$J = w_1 e_k^2 + w_2 \delta_k^2, \tag{12}$$

$$-\delta_m \leq \delta \leq \delta_m. \tag{13}$$

Figures 2(a) and 2(b) show the block-diagram of the controllers and a list of all control parameters is given in Table I.

TABLE I
CONTROLLER PARAMETERS

Controller	Parameters
SMC	$\lambda = 1, k = 0.15, \Phi = 0.15$
SMC-Modified	$\lambda = 1, k = 0.3, \Phi = 5$
MPC	$w_1 = 1, w_2 = 8, \delta_m = \pi/6$

V. SIMULATIONS

A. Vehicle and tire model

For simulations, a more realistic nonlinear eight degree of freedom vehicle model [56] is constructed. The model considers the longitudinal, lateral, roll, and yaw motions as well as rotations of all four wheels. A combined-slip tire force model called ”The elliptic tire model” [60] calculates tire forces based on the longitudinal and the side-slip under each tire. The simulation model and the controllers are implemented in MATLAB Simulink for evaluation and comparison of different transition curves.

The parameters are summarized in Table II. The parameters of the four-wheel model, including the elliptic tire, are matched to the bicycle and bicycle-roll models described in this document.

TABLE II
VEHICLE PARAMETERS

Parameter	Value [Unit]	Parameter	Value [Unit]
m	845.5 [kg]	$C_{\delta_{\phi f}}$	0.01
I_x	350 [kg.m^2]	$C_{\delta_{\phi r}}$	0.01
I_z	1490 [kg.m^2]	C_{ϕ_f}	-3200 [N/rad]
C_{α_f}	52000 [N/rad]	C_{ϕ_r}	0 [N/rad]
C_{α_r}	64000 [N/rad]	R_{w_i}	0.35 [m]
C_{T_f}	0.4 [m]	c_ϕ	1700 [Nm.s/rad]
C_{T_r}	0.4 [m]	k_ϕ	26612 [Nm/rad]
C_{β_f}	-0.4 [s]	a_1	0.909 [m]
C_{β_r}	-0.1 [s]	a_2	1.436 [m]

B. Reference Track

Based on the defined thresholds and the paths studied in [50] and [61], a reference track was designed using circular arcs to engulf the effects of motion sickness. The minimum radius (R_{min}) was 43m, calculated based on a passenger car (Chevrolet Corvette) traveling at 60 km/h(V) with a base(b)-to-height(h) ratio of 0.6584 using the overturning ratio Equation (14) [62]:

$$\frac{V^2}{gR_{min}} \leq \frac{(b/2)}{h}. \tag{14}$$

$$x = Rcos(t), \tag{15}$$

$$y = Rsin(t), \tag{16}$$

$$R^2 = (x-h)^2 + (y-k)^2. \tag{17}$$

Using Equations (14, 15, 16 and 17), the reference track was originated, as illustrated in Figure 3. The results shown in Figure 4 verify the reference track as the ”worst path”. As it acts in accordance with the five thresholds, summarised below:

- Reference track produces disruptive and abrupt lateral accelerations in excess of the discomfort range of $5m/s^2$.

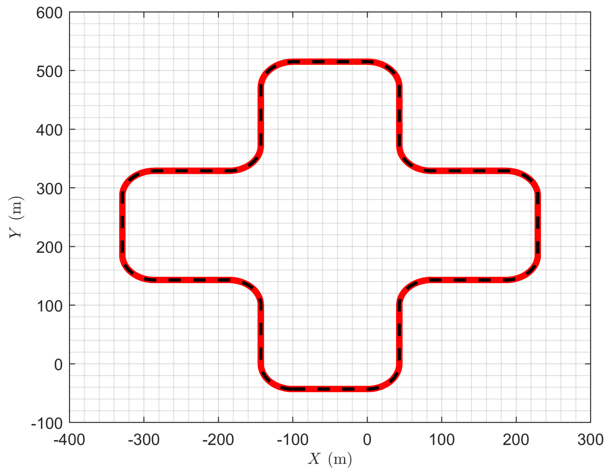

Fig. 3. Reference track generated using [15][16][17]

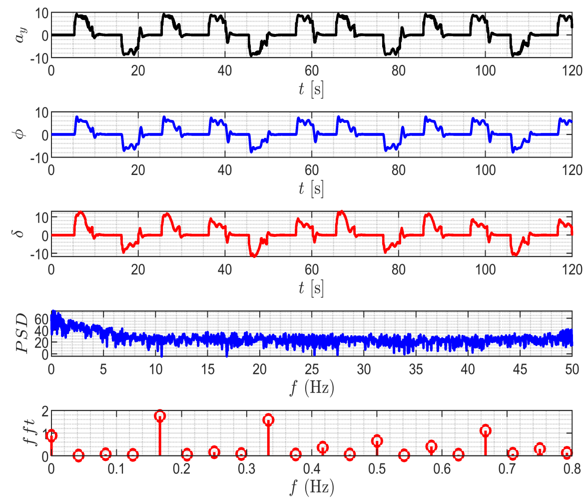

Fig. 4. Reference track results for lateral acceleration(m/s^2), roll oscillations, steering angle(degrees), PSD(dB/Hz) and FFT(m/s^2).

- The frequency spectrum produces high-magnitude low-frequency lateral accelerations. Based on frequency response in Figure 4, the power spectral density (PSD) value was the highest at frequencies below $1Hz$ ($60-70dB/Hz$), about $40dB/Hz$ higher than PSD values at frequencies greater than $1Hz$. Frequency can be further evaluated by zooming into the critical frequency range of $0.1Hz-0.2Hz$. A Fast Fourier Transform (FFT) of lateral acceleration has its highest magnitude at frequency $0.16Hz$ clocking a magnitude of $1.8m/s^2$, which is regarded as the peak frequency of sickness [5], making motion sickness in this path inevitable.
- Lateral acceleration and roll oscillations are in phase at all times.
- Abrupt and discontinuous changes in velocity and steering input are observed.
- The Path has 10 turns in alternating directions.

C. Transition Curves

Clothoids have been regularly used for road design or path planning [63]. However, Clothoids proved inefficient due to not having a closed-form representation [61], making them to be computationally slower than required. The need for computationally efficient curves led to designing paths using parametric curves such as vector-valued parametric splines for efficient planning used on differential robots [48], [64], [65], [66], [67] and [68]. Another form of parametric curve extensively used for path planning or path smoothing [50] and [69] are Bezier curves utilized in semi-structured environments. Research using Bezier has also been extended to trajectory generation in urban environments [70]. Later on, [71] proposed using B-spline curves compared to Bezier, suggesting that B-spline curves produced more realistic velocities and accelerations for physical systems. In a more recent study [61], the proposed continuous path smoothing algorithm for a car-like robot utilized B-spline curves. It was shown that steering behaviour produced by the algorithm mimicked the steering behaviour of a human very precisely. Parametric curves are utilized in the present study to investigate the impact on motion sickness as these curves are currently the most used path planning tools available.

- Parametric Cubic (Hermite) Curves are defined by four blending functions shown below:

$$F1 = 2u^3 - 3u^2 + 1, \tag{18}$$

$$F2 = -2u^3 + 3u^2, \tag{19}$$

$$F3 = u^3 - 2u^2 + u, \tag{20}$$

$$F4 = u^3 - u^2. \tag{21}$$

The Blending functions (18), (19), (20) and (21) are defined using a parameter u which ranges from 0 to 1 over the whole curve. where P(0) and P(1) are the starting and ending points of the curves respectively. The complete parametric curve equation is given as follows:

$$C(u) = P(0)F1 + P(1)F2 + \dot{P}(0)F3 + \dot{P}(1)F4. \tag{22}$$

- Bezier Curves are defined using the nth order based on the Equation (23):

$$C(u) = \sum_{i=0}^{n} B_{n,i}(u)P_i, \tag{23}$$

The blending functions are defined using the Binomial expansion given by the Equation (24):

$$B_{n,i}(u) = \frac{n!}{i!(n-i)!}u^i(1-u)^{n-i}. \tag{24}$$

The advantage of using Bezier curves is that arbitrary points can be selected to define the path, but at the cost of increasing the order of the curve, making the equation of the curve more complex whilst having only global control over the track/path.

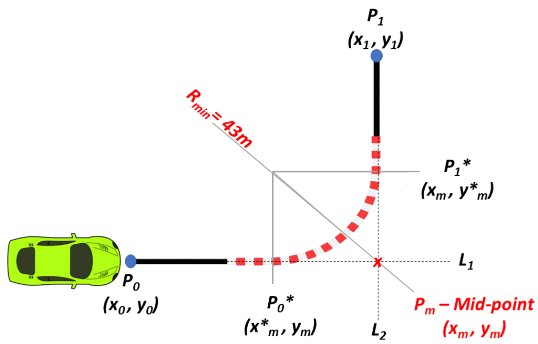

Fig. 5. Point selection Scheme for all topologies used in simulating ergonomic paths.

- B-Spline curves define a large Curve into smaller segments by using a knot vector t_i, and the blending functions are defined using the Basis function defined in Equation (25):

$$N_{i,k}(u) = \frac{[u - t_i]}{[t_{i+k-1} - t_i]} N_{i,k-1}(u) + \frac{[t_{i+k} - u]}{t_{i+k} - t_{i+1}} N_{i+1,k-1}(u), \tag{25}$$

To simplify the Basis function calculation Cox-de Boor algorithms are used [72], which are either equal to a 1 or 0 depending upon their existence in the concerned segment, as shown below:

$$N_{i,0} \begin{cases} = 1 & \text{if } t_i \leq u \leq t_{i+1} \\ = 0 & \text{elsewhere,} \end{cases}$$

To complete the Basis function, the values of k and i need to be defined where k is the order of the curve. For continuity purposes, k is taken as 3 or 4 since a B-spline's continuity is defined by the property C^{k-2}. As for i it takes the range from 0 to n, where $n = p - 1$ and p is the number of control points defined on the path, so the overall B-spline function is simplified and shown in Equation (26):

$$C(u) = \sum_{i=0}^{n} N_{i,k}(u) P_i. \tag{26}$$

D. Point Selection Scheme and Algorithm

For comparison purposes identifying a general point selection scheme is important for each of the three topologies (3-pt, 4-pt and 5-pt) used in simulating the ergonomic paths. When selecting the co-ordinates the key element was to ensure symmetry between starting and ending points, which is why the following scheme illustrated in Figure 5 was adopted. If (x_0, y_0) and (x_1, y_1) are starting (P_0) and ending (P_1) points of a curve respectively, then extending two imaginary lines from each point along the axis at which the points exist (L1 and L2 in Figure 5) a perpendicular intersection is formed which is defined as the mid-point of the 3-pt topology (P_m).

For the 4-pt topology, the minimum radius calculated (43m) is divided by 2 as shown in Equation (27) to find the respective shift (Δ^*) to formulate the 4-pt topology;

$$\Delta^* = R_{min}/2 \tag{27}$$

$$x_m^* = x_m \mp \Delta^* \tag{28}$$

$$y_m^* = y_m \pm \Delta^* \tag{29}$$

Thereafter, the mid-point is shifted along x and y axis equally by Δ^* to break down P_m into two distinct points either side of the mid-point as shown in Equations (28) and (29), and are labelled as P_0* (x_m^*, y_m) and P_1* (x_m, y_m^*) in Figure 5. Therefore, the 4-pt topology is generated based on the points: P_0, P_0*, P_1* and P_1. Subsequently, for 5-pt topology the points used are P_0, P_0*, P_m, P_1* and P_1. This point selection scheme is used as a benchmark for all simulations.

For calculating the radius of a turn; firstly, the co-ordinates of the center of the circle are calculated using Equations (30) and (31) (X_c, Y_c) and then the Radius (R) for each curve is computed using Equation (32) [54].

$$X_c = X - \dot{Y}(\dot{X}^2 + \dot{Y}^2)/(\ddot{Y}\dot{X} - \ddot{X}\dot{Y}) \tag{30}$$

$$Y_c = Y + \dot{X}(\dot{X}^2 + \dot{Y}^2)/(\ddot{Y}\dot{X} - \ddot{X}\dot{Y}) \tag{31}$$

$$R = \sqrt{(x - x_c)^2 + (y - y_c)^2} \tag{32}$$

The points and equations are then employed to calculate the path for each curve with its respective topologies, a general form of the path planning pseudo-code for the curves is seen on the next page. In the following section, the curves influence on motion sickness thresholds is compared, based on path characteristics and the controller[s].

Pseudo-code: Ergonomic path planning for all topologies
Input: P_0, P_1, P_m, P_0^* and P_1^*
Output: X, Y, X_C, Y_C and R
Procedure:
1. Selection of Curve
2. Selection of Topology
3. Calculation of Curve functions
4. Compute X, Y, X_C, Y_C and R

End Procedure

VI. Discussion

The results of the simulation are analyzed in this section.

- Curvature: To reduce the impact of motion sickness, curvature needs to be smooth (not abrupt) and above the minimum radius of rotation of $43m$. The only curve able to match these two conditions is the 3-pt B-spline curve, as seen in Figure 6. 3-pt Bezier and Hermite curves produce abrupt changes in the curvature and exceed the minimum radius limits in many turns of the path.
- Lateral acceleration magnitude: A path that produces lateral acceleration in the comfort range [29], whilst producing low amount of abrupt changes, produces a path with the lowest sickness. Ideal curve results shown

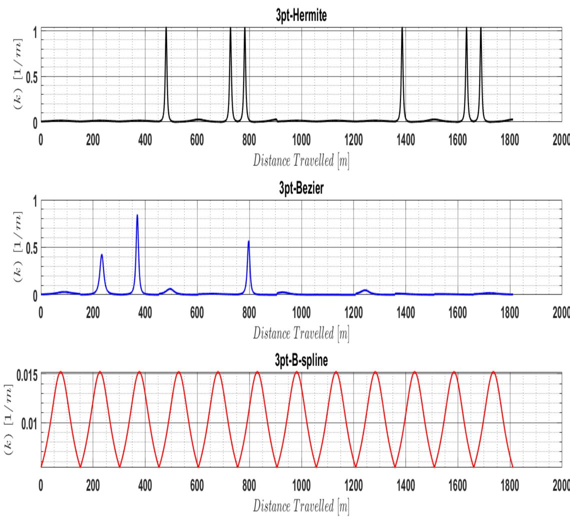

Fig. 6. Variation of curvature for 3-point defined transition curves, with Hermite(top), B-spline(bottom) and Bezier(middle) responses.

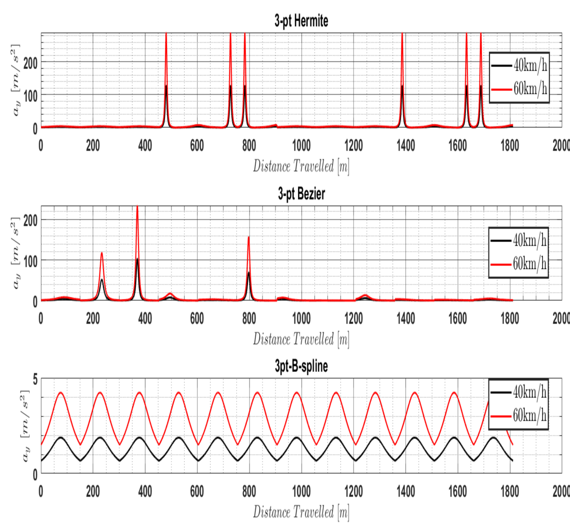

Fig. 7. Ideal lateral acceleration responses for the 3-point defined transition curves based on 2 different speeds (Black color graphs indicate vehicle speed equal to 40 km/h and red color graph indicates vehicle speed equal to 60 km/h.) .

in Figure 7 illustrate the only curve to produce such a response is the 3-pt B-spline curve (at only 40 km/h), with 3-pt B-spline at 60 km/h going marginally into the medium comfort zone. Moreover, when curves are passed through the controllers, 3-pt B-spline produces the least amount of abrupt changes and stays within the medium comfort range of lateral acceleration, as seen in Figure 8.

- Steering angle (controller[s]): The objective was analyzed by calculating the Root Mean Square Error (RMSE) of the lateral direction. A low RMSE signifies how well the controller follows the path, results in Table III show that SMC follows distinct features of curves, with 3-pt B-splines producing the lowest lateral error as compared to other curves. On the contrary, MPC responds equally to all curves whilst showing a certain steering improvement from the worst path to transition curves under investigation.

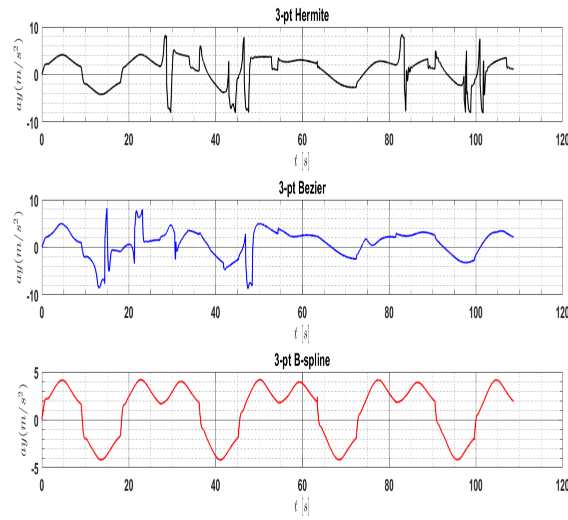

Fig. 8. Comparing three different curves used for defining a 3-point curve using curvature dependent controllers, with Hermite (top), Bezier (middle) and B-spline (bottom) responses.

TABLE III
RMSE VALUES OF LATERAL ERROR OF 3-PT CURVES AT 60KM/H

Controller type	"Worst Path"	Hermite	Bezier	B-spline
Curvature dependent (SMC)	n/a	17.11	17.13	1.126
Curvature independent (MPC)	0.435	0.254	0.254	0.254

Furthermore, Table IV indicates that the performance of MPC slightly deteriorates for a 4-pt Bezier curve by increasing RMSE by 7.5% only. As for 4-pt B-spline the performance deteriorates massively by increasing the RMSE by 95%.

In the case of SMC; RMSE values for 4-pt B-spline curves are higher by 88% as compared to 3-pt B-splines curves. On the contrary, a 4-pt Bezier curve simulated with SMC produced a RMSE value lower by 91% as compared to a 3-pt Bezier curve. Indicating that at higher orders Bezier curves perform better than B-splines for both sets of controllers.

Based on RMSE, it is recommended to use SMC only with 3-pt B-spline curves, while for MPC it does not matter which curve to use, as all curves produce identical results. However, it is recommended to use 3-pt topology for all curves, as they perform overall better than 4 or 5-pt curve topologies.

TABLE IV
RMSE VALUES OF LATERAL ERROR OF 4-PT CURVES AT 60KM/H

Controller type	Hermite	Bezier	B-spline
Curvature dependent (SMC)	n/a	1.397	9.744
Curvature independent (MPC)	n/a	0.273	5.32

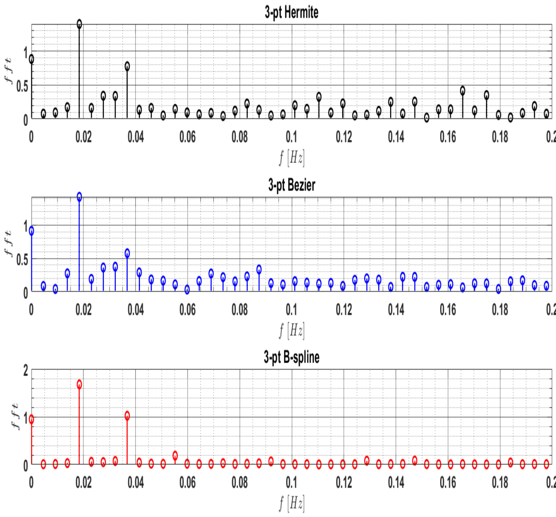

Fig. 9. Comparing lateral acceleration frequency response of a 3-point B-spline(top) against a 3-point Bezier(middle) and Hermite(bottom) curve using a curvature dependent controller.

- Frequency spectrum of lateral acceleration magnitude: To eliminate motion sickness the main task is to minimize the magnitude of lateral acceleration at the peak sickness frequency of $0.16Hz$. All of the studied curves are able to successfully suppress that particular magnitude in their frequency spectrum analysis, as seen in Figure 9.
Further, the Root Mean Square (RMS) values of each curve were compared in the frequency range of $0-1Hz$ [73], as illustrated in Table V.

TABLE V
RMS VALUES OF FFT (LATERAL ACCELERATION) AT 60 KM/H

	"Worst Path"	Hermite	Bezier	B-spline
3pt	0.0913	0.0216	0.0203	0.0201
4pt	n/a	n/a	0.021	0.0257

The results in Table V indicate how all transition curves perform better than the "Worst path" by decreasing the magnitude by a massive 76%. Moreover, 3-pt B-spline produces the lowest magnitudes as compared to 3 or 4-pt Bezier and Hermite curves. Indicating 3-pt B-spline not only suppresses the peak sickness frequency magnitude but also produces overall lower magnitudes of lateral acceleration in the motion sickness frequency range.
- Phase: No phase difference between the roll and lateral acceleration is observed using different transition curves under various scenarios. Hence, the phase threshold was compromised in this study with regards to motion sickness.
However, when the curves were tested for a lane-changing manoeuvre, it was noticed that a phase difference of 29 degrees existed, as seen in Figure 10. This indicates that lane changing manoeuvre as compared to a turning manoeuvre is a path which is less susceptible to motion sickness mainly due to two reasons; 1) lower exposure time means lower motion sickness dosage values (MSDV) as suggested in [20], [21], and 2) the presence of a phase difference between roll and lateral accelerations [22].

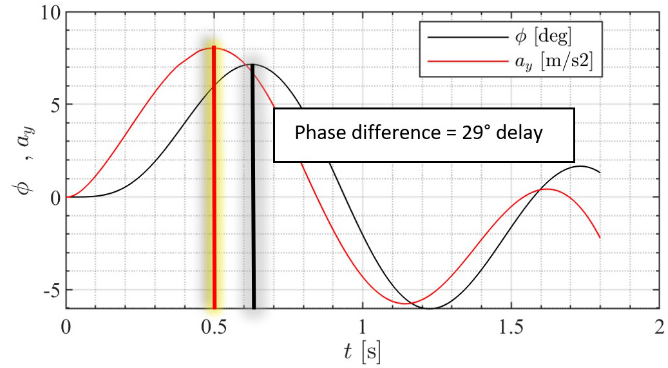

Fig. 10. Response of the lane changing manoeuvre due to our proposed B-spline curve using the controller.

Overall, 3-pt B-spline responses prove to be the best transition curve to address motion sickness thresholds as compared to Bezier (3/4/5-pt) or Hermite curves, based on the point selection scheme described earlier.

VII. FURTHER DISCUSSION

It is possible to constraint the lateral acceleration below the comfort range of $3.6m/s^2$ by defining the R_{min} to greater than or equal to 77m, calculated using Equation (33) at V = 60 Km/h, which can be obtained by optimizing the mid-point as shown in the algorithm below:

Algorithm: Mid-point optimization (3-pt B-splines)
Input: $P_0,\ P_1,\ and\ P_m$
Output: $OP-X_m$, $OP-Y_m$ and R_{min}
$C(u)=\sum_{i=0}^{2} N_{i,k}(u)P_i,\ R_{min}=0$
WHILE $R_{min}\leq 77$
  Calculate X, Y, X_C, Y_C and R
  R_{min}= R
  X_m= X_m-1 and Y_m= Y_m+1
END WHILE
$OP-X_m$= X_m and $OP-Y_m$= Y_m

$$V^2/3.6 = \ Maximum\ R_{(min)}. \tag{33}$$

Since, 3-pt B-splines are symmetrical, that means the exact same shift of the mid-point would apply to all the curves. It is important not to go higher than the maximum R_{min} found, as this increases the probability of lowering the overall variation in curvature, causing the curves to become too straight to be counted as a realistic turning manoeuvre. The comparison of results between a 3-pt B-spline (BS-06) and an optimized 3-pt B-spline (BS-06-OP) is shown in Table VI. Although, the path tracking error RMSE is higher for BS-06-OP as compared to BS-06, but in all other aspects of the thresholds it does far better, by reducing the average steering by 6.6%.

TABLE VI
COMPARISON BETWEEN A 3-PT B-SPLINE CURVE AND A 3-PT B-SPLINE OPTIMISED MID-POINT CURVE.

Thresholds	**BS-06**	**BS-06-OP**
RMSE	1.1261	1.8992
FFT$a_{y\,RMS}$	0.0201	0.0191
$\delta_{RMS}(degrees^{\circ})$	2.2656	2.1160
$a_{y\ RMS}$	2.9641	2.7642
a_y Peak	4.1980	3.7937

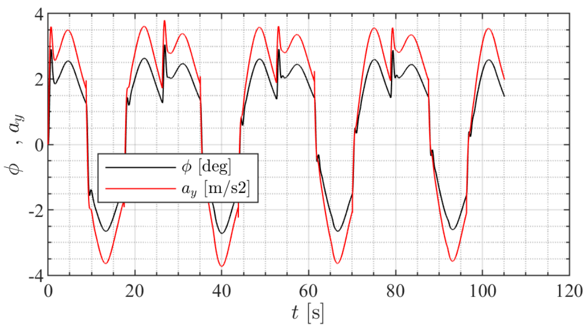

Fig. 11. Shows the lateral acceleration and roll for the BS-06-OP curve, when the vehicle is subjected to the reference track.

Also, producing lower magnitudes of lateral acceleration in the critical range of frequency of 0.1 Hz - 0.5 Hz by 5% and most importantly, reducing the lateral acceleration average and peak by 6.7% and 9.6% respectively.

However, BS-06-OP has a small trade-off (higher RMSE than BS-06), as it produces abrupt changes whenever two consecutive turns in the same direction are made (signifying a U-turn manoeuvre) as seen in Figure 11. It is recommended to further investigate this trade-off by using features like; 1)local control and 2) non-uniformity of B-splines, normally classified as NURBS (Non-Uniform Rational B-splines).

VIII. CONCLUSION

In summary, motion sickness thresholds in terms of vehicle dynamics were defined which were then used to design a worst path. Ergonomic paths were then studied by investigating the impact of using B-spline, Bezier, and Hermite as transition curves on motion sickness.

Results show that the transition curves utilized in this study reduce all of motion-sickness causing measures, except for the phase relationship between Roll and lateral acceleration.

Paths designed by 3-point B-spline curves proved to be the most effective in reducing motion sickness as compared to 4 or 5-point curves. Such curves produce continuity and allow subtle changes in lateral acceleration, curvature, turning radius, and steering angles, which in-turn allows gradual transition of a vehicle during the cornering manoeuvre. However, Bezier curves show improvement in the generated path when a higher order of the curve is used, but still as compared to a 3-pt B-spline curve they are not capable of producing lateral acceleration, roll and steering angles below the motion sickness thresholds. Hence, they are not suitable for the purpose of this study.

All transition curves successfully suppressed the lateral acceleration magnitude at peak sickness frequency of $0.16Hz$. Furthermore, 3-pt B-splines produced the lowest RMS values in the low-frequency range $(0-1Hz)$, indicating that transition curves like B-spline, Bezier, and Hermite effectively reduce the impact of low frequency on motion sickness in passengers.

SMC produced the best responses for a 3-point B-spline curve in terms of producing smooth, continuous, subtle changes in lateral acceleration and steering angles as the speed of the vehicle was increased from 40 km/h to 60 km/h. On the other hand, MPC does not present distinct features of the curves in the responses. Therefore, they produce almost identical results for all three transition curves in terms of lateral acceleration. Moreover, resulting in sharper turns and higher lateral accelerations than SMC.

The phase relationship between roll and lateral accelerations could not be altered using the studied transition curves. Further investigation into non-uniform rational B-spline (NURBS) curves is recommended to address the phase threshold of motion sickness. However, it was observed that a lane-changing manoeuvre produces a phase shift between the roll and lateral acceleration of 29 degrees, indicating that a lane-changing manoeuvre is less susceptible to motion sickness as compared to a cornering manoeuvre.

Transition curves used in this study are open uniform and do not address two key characteristics of a B-spline curve; which are (1) local control and (2) non-uniformity. These two are of much interest to the investigation of further optimizing the thresholds of motion sickness defined in this study. In conclusion, this investigation determines that a 3-pt B-spline is the most promising curve to minimize motion sickness by addressing the defined thresholds and can be tracked with high accuracy by either MPC or SMC.

REFERENCES

[1] S. O.-R. A. V. S. Committee *et al.*, "Taxonomy and definitions for terms related to on-road motor vehicle automated driving systems," *SAE Standard J*, vol. 3016, pp. 1–16, 2014.

[2] T. E. Trimble, R. Bishop, J. F. Morgan, M. Blanco, *et al.*, "Human factors evaluation of level 2 and level 3 automated driving concepts: Past research, state of automation technology, and emerging system concepts," 2014.

[3] M. Elbanhawi, M. Simic, and R. Jazar, "In the passenger seat: investigating ride comfort measures in autonomous cars," *IEEE Intelligent Transportation Systems Magazine*, vol. 7, no. 3, pp. 4–17, 2015.

[4] J. Weyer, R. D. Fink, and F. Adelt, "Human–machine cooperation in smart cars. an empirical investigation of the loss-of-control thesis," *Safety science*, vol. 72, pp. 199–208, 2015.

[5] C. Diels and J. E. Bos, "Self-driving carsickness," *Applied ergonomics*, vol. 53, pp. 374–382, 2016.

[6] C. G. L. Bianco, "Minimum-jerk velocity planning for mobile robot applications," *IEEE Transactions on Robotics*, vol. 29, no. 5, pp. 1317–1326, 2013.

[7] H. Bellem, B. Thiel, M. Schrauf, and J. F. Krems, "Comfort in automated driving: An analysis of preferences for different automated driving styles and their dependence on personality traits," *Transportation research part F: traffic psychology and behaviour*, vol. 55, pp. 90–100, 2018.

[8] Y. Morales, N. Kallakuri, K. Shinozawa, T. Miyashita, and N. Hagita, "Human-comfortable navigation for an autonomous robotic wheelchair," in *2013 IEEE/RSJ International Conference on Intelligent Robots and Systems*. IEEE, 2013, pp. 2737–2743.

[9] N. Mohajer, S. Nahavandi, H. Abdi, and Z. Najdovski, "Enhancing passenger comfort in autonomous vehicles through vehicle handling analysis and optimization," *IEEE Intelligent Transportation Systems Magazine*, 2020.

[10] J. E. Bos, W. Bles, and E. L. Groen, "A theory on visually induced motion sickness," *Displays*, vol. 29, no. 2, pp. 47–57, 2008.

[11] P. Feenstra, J. E. Bos, and R. N. van Gent, "A visual display enhancing comfort by counteracting airsickness," *Displays*, vol. 32, no. 4, pp. 194–200, 2011.

[12] D. Tal, A. Gonen, G. Wiener, R. Bar, A. Gil, Z. Nachum, and A. Shupak, "Artificial horizon effects on motion sickness and performance," *Otology & Neurotology*, vol. 33, no. 5, pp. 878–885, 2012.

[13] P. S. Cowings, *Effects of command and control vehicle (C2V) operational environment on soldier health and performance*. Army research lab aberdeen proving ground md, 1999.

[14] K. Kato and S. Kitazaki, "Improvement of ease of viewing images on an in-vehicle display and reduction of carsickness," SAE Technical Paper, Tech. Rep., 2008.

[15] K. Money, "Signs and symptoms of motion sickness and its basic nature," in *Mechanisms and control of emesis*. John Libbey Eurotext Montrouge, 1992, pp. 177–184.

[16] J. T. Reason and J. J. Brand, *Motion sickness.* Academic press, 1975.

[17] G. E. Riccio and T. A. Stoffregen, "An ecological theory of motion sickness and postural instability," *Ecological psychology*, vol. 3, no. 3, pp. 195–240, 1991.

[18] J. E. Bos, "Nuancing the relationship between motion sickness and postural stability," *Displays*, vol. 32, no. 4, pp. 189–193, 2011.

[19] R. S. Kennedy and K. M. Stanney, "Postural instability induced by virtual reality exposure: Development of a certification protocol," *International Journal of Human-Computer Interaction*, vol. 8, no. 1, pp. 25–47, 1996.

[20] M. Griffin and M. Newman, "An experimental study of low-frequency motion in cars," *Proceedings of the Institution of Mechanical Engineers, Part D: Journal of Automobile Engineering*, vol. 218, no. 11, pp. 1231–1238, 2004.

[21] J. A. Joseph and M. J. Griffin, "Motion sickness: Effect of the magnitude of roll and pitch oscillation," *Aviation, space, and environmental medicine*, vol. 79, no. 4, pp. 390–396, 2008.

[22] ——, "Motion sickness from combined lateral and roll oscillation: effect of varying phase relationships," *Aviation, space, and environmental medicine*, vol. 78, no. 10, pp. 944–950, 2007.

[23] M. Turner and M. J. Griffin, "Motion sickness in public road transport: the effect of driver, route and vehicle," *Ergonomics*, vol. 42, no. 12, pp. 1646–1664, 1999.

[24] M. L. Jones, V. C. Le, S. M. Ebert, K. H. Sienko, M. P. Reed, and J. R. Sayer, "Motion sickness in passenger vehicles during test track operations," *Ergonomics*, vol. 62, no. 10, pp. 1357–1371, 2019.

[25] F. Savona, A. M. Stratulat, E. Diaz, V. Honnet, G. Houze, P. Vars, S. Masfrand, V. Roussarie, and C. Bourdin, "The influence of lateral, roll and yaw motion gains on driving performance on an advanced dynamic simulator," in *Proceedings of the sixth international conference on advances in system simulation*. Citeseer, 2014, pp. 113–119.

[26] A. S. Kilinç and T. Baybura, "Determination of minimum horizontal curve radius used in the design of transportation structures, depending on the limit value of comfort criterion lateral jerk," in *TS06G-Engineering Surveying, Machine Control and Guidance*, 2012.

[27] K. K. Dixon and J. W. Rohani, "Spr 641: Methodologies for estimating advisory curve speeds on oregon highways," *Salem, OR: Oregon Department of Transportation*, 2008.

[28] A. P. Voigt, D. W. Fenno, and D. W. Borchardt, *Evaluation of vehicle speeds on freeway-to-freeway connector ramps in Houston*. Texas Transportation Institute, Texas A & M University System, 2003, vol. 4318, no. 1.

[29] J. Xu, K. Yang, Y. Shao, and G. Lu, "An experimental study on lateral acceleration of cars in different environments in sichuan, southwest china," *Discrete Dynamics in nature and Society*, vol. 2015, 2015.

[30] P. Green, "Motion sickness and concerns for self-driving vehicles: a literature review," *Tech. Rep. UMTRI-2016), Ann Arbor, MI Univ. Michigan Transp. Res. Institute.*, 2016.

[31] J. Treleaven, J. Battershill, D. Cole, C. Fadelli, S. Freestone, K. Lang, and H. Sarig-Bahat, "Simulator sickness incidence and susceptibility during neck motion-controlled virtual reality tasks," *Virtual Reality*, vol. 19, no. 3-4, pp. 267–275, 2015.

[32] M. Klüver, C. Herrigel, C. Heinrich, H.-P. Schöner, and H. Hecht, "The behavioral validity of dual-task driving performance in fixed and moving base driving simulators," *Transportation research part F: traffic psychology and behaviour*, vol. 37, pp. 78–96, 2016.

[33] B. Keshavarz and H. Hecht, "Validating an efficient method to quantify motion sickness," *Human factors*, vol. 53, no. 4, pp. 415–426, 2011.

[34] B. Aykent, F. Merienne, D. Paillot, and A. Kemeny, "The role of motion platform on postural instability and head vibration exposure at driving simulators," *Human movement science*, vol. 33, pp. 354–368, 2014.

[35] R. S. Kennedy, J. Drexler, and R. C. Kennedy, "Research in visually induced motion sickness," *Applied ergonomics*, vol. 41, no. 4, pp. 494–503, 2010.

[36] B. S. Institution, *Measurement and evaluation of human exposure to whole-body mechanical vibration and repeated shock*. BSI, 1987.

[37] I. O. for Standardization, "Mechanical vibration and shock: evaluation of human exposure to whole-body vibration. part 1, general requirements–amendment1 iso 2631-1: 1997/amd 1: 2010," 2010.

[38] Z. Htike, G. Papaioannou, E. Velenis, and S. Longo, "Motion planning of self-driving vehicles for motion sickness minimisation," in *2020 European Control Conference (ECC)*. IEEE, 2020, pp. 1719–1724.

[39] T. Wiederkehr and F. Altpeter, "Review of motion sickness evaluation methods and their application to simulation technology," *SIMPACK News, July*, 2013.

[40] J. Karjanto, N. M. Yusof, C. Wang, J. Terken, F. Delbressine, and M. Rauterberg, "The effect of peripheral visual feedforward system in enhancing situation awareness and mitigating motion sickness in fully automated driving," *Transportation research part F: traffic psychology and behaviour*, vol. 58, pp. 678–692, 2018.

[41] S. Salter, C. Diels, D. Thake, *et al.*, "Motion sickness prediction device for automated vehicles," *Int J Mech Produc Eng*, vol. 7, pp. 68–74, 2019.

[42] C. Strychacz, E. Viirre, and S. Wing, "The use of eeg to measure cerebral changes during computer-based motion-sickness-inducing tasks," in *Biomonitoring for Physiological and Cognitive Performance during Military Operations*, vol. 5797. International Society for Optics and Photonics, 2005, pp. 139–148.

[43] C.-T. Lin, S.-F. Tsai, H.-C. Lee, H.-L. Huang, S.-Y. Ho, and L.-W. Ko, "Motion sickness estimation system," in *The 2012 International Joint Conference on Neural Networks (IJCNN)*. IEEE, 2012, pp. 1–6.

[44] L.-W. Ko, C.-S. Wei, S.-A. Chen, and C.-T. Lin, "Eeg-based motion sickness estimation using principal component regression," in *International Conference on Neural Information Processing*. Springer, 2011, pp. 717–724.

[45] C.-T. Lin, S.-F. Tsai, and L.-W. Ko, "Eeg-based learning system for online motion sickness level estimation in a dynamic vehicle environment," *IEEE transactions on neural networks and learning systems*, vol. 24, no. 10, pp. 1689–1700, 2013.

[46] N. Kamiji, Y. Kurata, T. Wada, and S. Doi, "Modeling and validation of carsickness mechanism," in *SICE Annual Conference 2007*. IEEE, 2007, pp. 1138–1143.

[47] F. A. Cheein and G. Scaglia, "Trajectory tracking controller design for unmanned vehicles: A new methodology," *Journal of Field Robotics*, vol. 31, no. 6, pp. 861–887, 2014.

[48] B. Lau, C. Sprunk, and W. Burgard, "Kinodynamic motion planning for mobile robots using splines," in *2009 IEEE/RSJ International Conference on Intelligent Robots and Systems*. IEEE, 2009, pp. 2427–2433.

[49] S. A. Roth and P. Batavia, "Evaluating path tracker performance for outdoor mobile robots," in *Automation Technology for Off-Road Equipment Proceedings of the 2002 Conference*. American Society of Agricultural and Biological Engineers, 2002, p. 388.

[50] K. Yang and S. Sukkarieh, "An analytical continuous-curvature path-smoothing algorithm," *IEEE Transactions on Robotics*, vol. 26, no. 3, pp. 561–568, 2010.

[51] R. N. Jazar, "Mathematical theory of autodriver for autonomous vehicles," *Journal of Vibration and Control*, vol. 16, no. 2, pp. 253–279, 2010.

[52] H. Marzbani, A. Mohd Harithuddin, M. Simic, M. Fard, and G. Nakhaie Jazar, "Steady-state dynamic steering," in *Smart Digital Futures 2014 (SDF-14)*. IOS Press, 2014, pp. 493–504.

[53] H. Marzbani, H. Khayyam, C. N. TO, . V. Quoc, and R. N. Jazar, "Autonomous vehicles: Autodriver algorithm and vehicle dynamics," *IEEE Transactions on Vehicular Technology*, vol. 68, no. 4, pp. 3201–3211, 2019.

[54] R. N. Jazar, *Advanced vehicle dynamics*. Springer, 2019.

[55] H. Marzbani, R. N. Jazar, and M. Fard, "Steady-state vehicle dynamics," in *Nonlinear approaches in engineering applications*. Springer, 2015, pp. 3–30.

[56] S. Milani, H. Khayyam, H. Marzbani, W. Melek, N. L. Azad, and R. N. Jazar, "Smart autodriver algorithm for real-time autonomous vehicle trajectory control," *IEEE Transactions on Intelligent Transportation Systems*, 2020.

[57] S. Milani, H. Marzbani, A. Khazaei, and R. N. Jazar, “Vehicles are lazy: On predicting vehicle transient dynamics by steady-state responses,” in *Nonlinear Approaches in Engineering Applications*. Springer, 2020, pp. 3–38.

[58] R. N. Jazar, *Vehicle dynamics: theory and application*. Springer, Cham, 2017.

[59] S. Tajeddin, “Mpsee (https://www.mathworks.com/matlabcentral/fileexchang mpsee),” 2020.

[60] S. Milani, H. Marzbani, A. Khazaei, M. Simic, and R. N. Jazar, “Elliptical combined-slip tire model in vehicle dynamics,” in *Innovation in Medicine and Healthcare Systems, and Multimedia*. Springer, 2019, pp. 457–468.

[61] M. Elbanhawi, M. Simic, and R. Jazar, “Improved manoeuvring of autonomous passenger vehicles: simulations and field results,” *Journal of Vibration and Control*, vol. 23, no. 12, pp. 1954–1983, 2017.

[62] P. Mohan, *GATE 2020 Civil Engineering Guide with 10 Practice Sets (6 in Book + 4 Online) 7th edition*. Disha publications, 2019.

[63] H. Marzbani, R. N. Jazar, and M. Fard, “Better road design using clothoids,” in *Sustainable automotive technologies 2014*. Springer, 2015, pp. 25–40.

[64] U.-Y. Huh and S.-R. Chang, “Ag 2 continuous path-smoothing algorithm using modified quadratic polynomial interpolation,” *International Journal of Advanced Robotic Systems*, vol. 11, no. 2, p. 25, 2014.

[65] E. Magid, D. Keren, E. Rivlin, and I. Yavneh, “Spline-based robot navigation,” in *2006 IEEE/RSJ International Conference on Intelligent Robots and Systems*. IEEE, 2006, pp. 2296–2301.

[66] J. Connors and G. Elkaim, “Analysis of a spline based, obstacle avoiding path planning algorithm,” in *2007 IEEE 65th Vehicular Technology Conference-VTC2007-Spring*. IEEE, 2007, pp. 2565–2569.

[67] S. Gulati, C. Jhurani, B. Kuipers, and R. Longoria, “A framework for planning comfortable and customizable motion of an assistive mobile robot,” in *2009 IEEE/RSJ International Conference on Intelligent Robots and Systems*. IEEE, 2009, pp. 4253–4260.

[68] K. Jolly, R. S. Kumar, and R. Vijayakumar, “A bezier curve based path planning in a multi-agent robot soccer system without violating the acceleration limits,” *Robotics and Autonomous Systems*, vol. 57, no. 1, pp. 23–33, 2009.

[69] K. Yang, S. Moon, S. Yoo, J. Kang, N. L. Doh, H. B. Kim, and S. Joo, “Spline-based rrt path planner for non-holonomic robots,” *Journal of Intelligent & Robotic Systems*, vol. 73, no. 1-4, pp. 763–782, 2014.

[70] J. Pérez, J. Godoy, J. Villagrá, and E. Onieva, “Trajectory generator for autonomous vehicles in urban environments,” in *2013 IEEE International Conference on Robotics and Automation*. IEEE, 2013, pp. 409–414.

[71] J. Pan, L. Zhang, and D. Manocha, “Collision-free and smooth trajectory computation in cluttered environments,” *The International Journal of Robotics Research*, vol. 31, no. 10, pp. 1155–1175, 2012.

[72] C. De Boor, “On calculating with b-splines,” *Journal of Approximation theory*, vol. 6, no. 1, pp. 50–62, 1972.

[73] B. E. Donohew and M. J. Griffin, “Motion sickness: effect of the frequency of lateral oscillation,” *Aviation, Space, and Environmental Medicine*, vol. 75, no. 8, pp. 649–656, 2004.

Muhammad Rehan Siddiqi Received his B.Sc. from Ajman University, U.A.E and his MEM from University of Wollongong, Dubai, U.A.E. He is currently doing his PhD at RMIT University, Melbourne, Australia. His most current research interest is understanding the impact of motion sickness in AV. He has published several articles including a book to his name in the field of engineering studies.

Sina Milani Received his B.Sc. from K.N.Toosi University of Technology, Tehran, Iran and his M.Sc. from Middle East Technical University, Ankara, Turkey. He is currently a PhD candidate at RMIT University, Melbourne, Australia. His research interests include Vehicle Dynamics and Control, Vehicle Safety Systems, Autonomous Driving, Robotics. He has been author and coauthor of a number of publications on mechanical engineering applications.

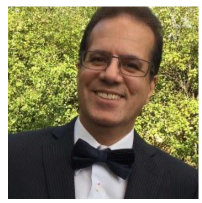

Reza N. Jazar Received the masters degree in robotics from Tehran Polytechnic, in 1990, and the Ph.D. degree in nonlinear dynamics and applied mathematics from the Sharif University of Technology, in 1997. He is currently a Professor of mechanical engineering. He is also a Specialist in classical and nonlinear dynamic systems and has extensive experience in the field of vehicle dynamics and mathematical modeling. He has worked in several universities worldwide, and through his years of work experience, he has formulated many theorems, innovative ideas, and discoveries in classical dynamics, robotics, control, and nonlinear vibrations. Razi acceleration, theory of time derivative, order-free transformations, caster theory, autodriver algorithm, floating-time method, energy-rate method, and RMS Optimization method are some of his discoveries and innovative ideas. He has authored 15 books all among the most prestigious publications in their fields.

Hormoz Marzabani Received his PhD in Mechanical Engineering from RMIT University, Melbourne, Australia in 2015. He is working as a Lecturer since 2015. His main research interests include the field of dynamics, vibration, vehicle dynamics, and autonomous land vehicles. The autodriver algorithm that is a novel mathematical theory for autonomous driving of the cars considering the vehicle dynamics, constraints, and mathematics of the road ahead is his major field of study and contribution.